New Phytologist

Research

A CBL-interacting protein kinase ZmCIPK12 confers salt tolerance in maize

Jian Li[1,2], Xinyun Han[1], Yiru Wang[1], Yangsong Chen[1], Xunji Chen[1,3], Yuhang Guo[1,4], Zhen Chen[1], Xiaodong Wang[1,5], Quansheng Huang[3], Chun Liu[1], Wenyue Wang[1], Rui Li[1], Zhifeng Chen[1], Yang Qin[1], Jian Hua[6] and Jun Zheng[1]

[1]State Key Laboratory of Crop Gene Resources and Breeding, Institute of Crop Sciences, Chinese Academy of Agricultural Sciences, Beijing, 100081, China; [2]State Key Laboratory of Crop Genetics & Germplasm Enhancement and Utilization, College of Agriculture, Nanjing Agricultural University, Nanjing, 210095, China; [3]Institute of Nuclear Technology and Biotechnology, Xinjiang Academy of Agriculture/Xinjiang Key Laboratory of Crop Biotechnology, Urumqi, 830091, China; [4]College of Agronomy and Biotechnology, China Agricultural University, Beijing, 100193, China; [5]Institute of Food Crops, Xinjiang Academy of Agricultural Sciences, Urumqi, 830091, China; [6]Plant Biology Section, School of Integrative Plant Science, Cornell University, Ithaca, NY 14853, USA

Authors for correspondence:
Jun Zheng
Email: zhengjun02@caas.cn

Jian Hua
Email: jh299@cornell.edu

Received: *11 August 2025*
Accepted: *10 September 2025*

New Phytologist (2025)
doi: 10.1111/nph.70602

Key words: cell wall, maize, phosphorylation, salt tolerance, *ZmCIPK12*.

Summary

- Increasing salt stress tolerance is crucial for sustainable agriculture, including the production of the major crop maize (*Zea mays*). However, the molecular mechanism of salt stress tolerance remains largely unknown in maize.
- Here, we studied the function and mechanism of the maize *calcineurin B-Like-interacting protein kinase 12* (*ZmCIPK12*) in salt stress tolerance using mutant study, protein–protein interaction assay, protein biochemical characterization, and transcriptome analysis.
- We show that the loss of *ZmCIPK12* function reduces salt tolerance in maize, while its overexpression increases salt tolerance. ZmCIPK12 interacts with the maize-soluble inorganic pyrophosphatase 4 (ZmPPase4) and inhibits its degradation. The loss of function of *ZmPPase4*, similar to that of *ZmCIPK12*, causes salt stress susceptibility in maize. In addition, the *ZmCIPK12* and *ZmPPase4* affect cell wall thickness under salt stress, which likely contributes to salt tolerance.
- Taken together, this study shows that ZmCIPK12 enhances salt tolerance likely through stabilizing ZmPPase4 and regulating cell wall thickness. It broadens our understanding of the plant salt tolerance mechanism and provides potential targets for improving salt tolerance in maize.

Introduction

Soil salinization is a major abiotic stress, damaging plant growth and global food security (Zhao *et al.*, 2020). Forty-five million hectares of irrigated land are negatively affected by salinity (Munns & Tester, 2008). Maize is the most important C_4 crop, providing food and industrial materials world-wide. However, *c.* 70% of maize is cultivated in arid and semiarid regions globally, which are adversely impacted by salinity. The production of maize is significantly hampered by soil salinization (Cao *et al.*, 2023). Therefore, understanding the mechanisms of salt tolerance is essential for developing salt-tolerant maize cultivars.

Calcineurin B-Like (CBL)-interacting protein kinases are typical serine/threonine protein kinases that belong to the Snf1-related kinase 3 family (de la Torre *et al.*, 2013). *CIPK* genes play vital roles in regulating various biological processes in response to biotic and abiotic stresses, including salt stress in plants (Luan, 2009). Salt overly sensitive 1 (SOS1) localizes to the plasma membrane, late endosome/prevacuoles, and vacuoles, where it orchestrates critical roles in plant Na^+ extrusion and compartmentalization (Shi *et al.*, 2000; Ramakrishna *et al.*, 2025). *CIPK* is a part of the well-studied SOS pathway for salt tolerance in Arabidopsis (Zhu, 2016). Previous studies have shown that CBLs and CIPKs form protein complexes to trigger downstream salt responses (Zhang *et al.*, 2020). A CBL protein SOS3 (AtCBL4) specifically interacts with the C-terminal regulatory domain of a CIPK protein SOS2 (AtCIPK24), leading to the activation of the Na^+/H^+ antiporter SOS1, to increase Na^+ extrusion out of the cells from the cytoplasm to the apoplast for salt tolerance (Halfter *et al.*, 2000; Yang & Guo, 2018). Among the 43 putative *CIPK* genes in maize (Chen *et al.*, 2011), *ZmCIPK24a* and *ZmCIPK42* have been implicated in salt tolerance. The *zmcipk42* mutant exhibits impaired salt stress tolerance at the seedling stage, whereas *ZmCIPK42* overexpression (OE) in Arabidopsis confers enhanced salt resistance (X. Chen *et al.*, 2021). ZmCIPK24a is the closest homolog of Arabidopsis SOS2, and it interacts with ZmCBL4 and phosphorylates

ZmSOS1 to activate its Na^+-transporting activity (Zhou *et al.*, 2022). Whether or not other *CIPKs* are involved in salt tolerance in maize is unknown.

Soluble inorganic pyrophosphatase (sPPase) plays an essential function in cellular metabolism, such as the biosynthesis of sugars, nucleic acids and proteins (Segami *et al.*, 2018). sPPase

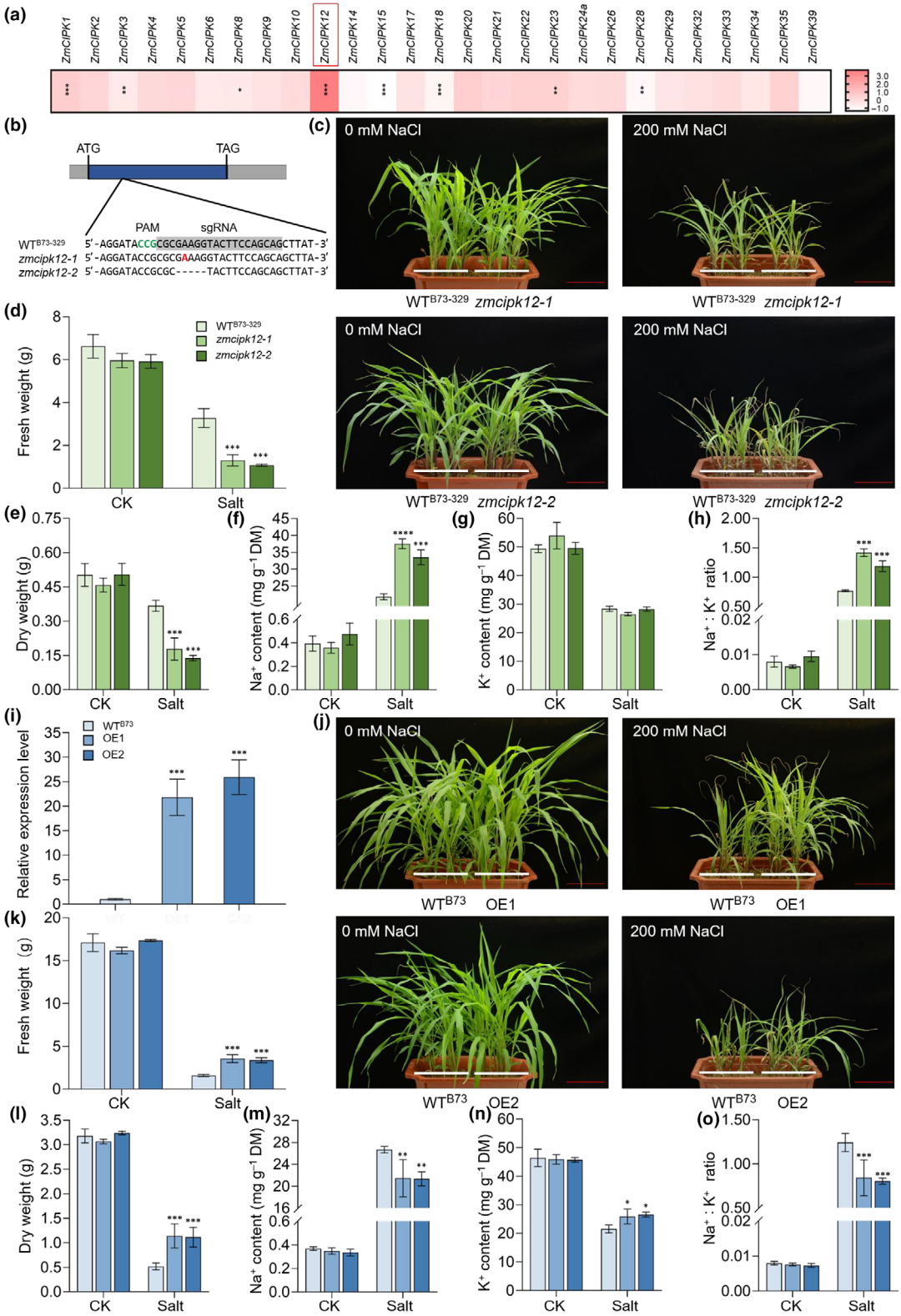

Fig. 1 Phenotypic analysis of wild-type (WT), *zmcipk12*, and *ZmCIPK12* overexpression (OE) plants under normal and salt treatment. (a) Transcriptomic analysis of *ZmCIPKs* in response to salt stress. The values represent the ratio of gene expression under salt treatment to that under normal conditions with a $\log_2$ transformation. Asterisks represent the statistical significance of differentially expressed genes (DEGs). (b) Two homozygous CRISPR/Cas9 knockout lines (*zmcipk12-1* and *zmcipk12-2*) with insertion or deletion in the target site of *ZmCIPK12*. The gene model and the WT sequence are shown at the upper panel. Protospacer adjacent motif (PAM) sequence is highlighted in green. Single-guide RNA (sgRNA) sequence is highlighted in gray. (c) Phenotypes of $WT^{B73\text{-}329}$, *zmcipk12-1*, and *zmcipk12-2* under normal and salt treatment. (d–h) Comparison of shoot fresh weight (d), dry weight (e), Na^+ content (f), K^+ content (g), and Na^+ : K^+ ratio (h) between $WT^{B73\text{-}329}$ and *zmcipk12* plants under normal and salt stress conditions. Three seedlings were collected for the assessment of indicators. Statistical significance was determined by a two-way ANOVA. (i) Relative expression level of *ZmCIPK12* OE lines. (j) Phenotypes of *ZmCIPK12* OE plants under normal and salt treatment conditions. (k–o) Comparison of shoot fresh weight (k), dry weight (l), Na^+ content (m), K^+ content (n), and Na^+ : K^+ ratio (o) under normal or NaCl treatment conditions. Five seedlings were collected for the assessment of indicators. Bars, 10 cm. Error bars show the mean ± SD (n = 3). Statistical significance was determined by one-way ANOVA or two-way ANOVA: *, $P < 0.05$; **, $P < 0.01$; ***, $P < 0.001$; ****, $P < 0.0001$. CK, control check.

catalyzes the catabolism of intracellular inorganic pyrophosphate (PPi) to provide a thermodynamic driving force and to avoid toxicity induced by high cytosolic PPi in cells. sPPases affect growth and development. Transmission electron microscopy (TEM) analysis reveals incomplete cell walls in the *fugu5-1 ppa1-1* double mutant lacking a vacuolar H^+-pyrophosphatase and a sPPase. The cell walls in *fugu5-1 ppa1-1* are severely weakened when compared to *fugu5-1*, suggesting a regulation of the cell wall by sPPase (Segami *et al.*, 2018). Very few *sPPase* genes have been reported to function in stress tolerance. Overexpressing an *sPPase* gene, ThPP1 of *Thellungiella halophila*, confers enhanced tolerance to alkali stress in rice (He *et al.*, 2017). An *osppa6* mutant generated by the clustered regularly interspaced short palindromic repeats (CRISPR) / Cas9 system is more sensitive to alkali stress (Wang *et al.*, 2019). Phosphorylation modification has been reported to regulate sPPase activity. The *Papaver rhoeas* calcium-dependent protein kinases 14 (PrCPK14) could phosphorylate Pr-p26.1a and Pr-p26.1b and modify their pyrophosphatase activity (Eaves *et al.*, 2017). However, whether or not *sPPases* regulate salt tolerance in plants is unknown.

Cell wall characteristics are associated with salt tolerance. The cell wall is one of the early sensors of salt stress and provides a physical barrier between the plasma membrane and the environment (Zhao *et al.*, 2021; Colin *et al.*, 2023). Previous research has identified over 70 gene families that are cell wall related in maize (Penning *et al.*, 2019). Inhibition of PAL gene transcription reduces lignin biosynthesis and secondary cell wall deposition in stems (Ye *et al.*, 2025). Peroxidase induces cell wall cross-linking, leading to cell wall thickening and stiffening (Zhao *et al.*, 2023). The cell wall is modified by the environment. Stress-induced reactive oxygen species elevates the expression of laccases through *microRNA408*, resulting in the accumulation of lignin and thickened cell walls in maize (Qin *et al.*, 2023). However, the mechanism influencing the cell wall under salt stress in maize remains largely unclear.

In this study, we report that the *zmcipk12* knockout lines were hypersensitive to salt stress while the *ZmCIPK12 OE* improved salt tolerance in maize. Furthermore, ZmCIPK12 interacts with ZmPPase4 and phosphorylates ZmPase4 to promote its stability. In addition, *ZmCIPK12* and *ZmPPase4* both positively regulate cell wall thickness under salt stress. These findings reveal new regulators of salt tolerance in maize and provide potential genetic targets for breeding salt-tolerant maize varieties.

Materials and Methods

Plant growth and treatments

The cultivation of the plants, as shown in Figs 1 and 4 (described later), was conducted using the following methodology. Seedlings were grown in pots (33 × 23 × 13 cm, length × width × depth) filled with vermiculite. The plants were treated with Hoagland's nutrient solution containing either 0 or 200 mM NaCl for 14 d after 8 d of normal growth. Maize seedlings were planted in a growth chamber at 28°C with a 16 h : 8 h, day : night period and a relative humidity of *c.* 60%.

RNA sequencing

Plant samples were processed at Beijing Qingke Biotechnology Co. Ltd (Beijing, China), for RNA extraction, purification, and library construction. The transcriptome sequencing was performed on the Hi-Seq Illumina platform. Genes identified by DESeq2 with $P < 0.05$ and $|\log_2(\text{fold change})| \geq 1$ were classified as differentially expressed for three biological replicates. Differentially expressed genes (DEGs) were analyzed using AgriGO (http://systemsbiology.cau.edu.cn/agriGOv2/index.php).

RNA isolation and quantitative RT-PCR analysis

Total RNA was extracted with the RNA Easy Fast Plant Tissue Kit (DP452; Tiangen, Beijing, China). The cDNA was synthesized using the PrimeScript™ FAST RT Reagent Kit with gDNA Eraser (RR092S; Takara Biomedical Technology (Beijing) Co. Ltd, Beijing, China). Quantitative real-time PCR (qRT-PCR) was performed using the TB Green® Premix Ex Taq™ II FAST qPCR (CN830A; Takara) on a 7300 Real-Time PCR System (Applied Biosystems, Foster City, CA, USA) following the manufacturer's protocols. *GAPDH* was used as an internal control. The primers used for qRT-PCR are listed in Supporting Information Table S1.

Generation of the CRISPR/Cas9 knockout lines

The *ZmCIPK12* knockout lines were generated using the CRISPR/Cas9 editing method as described previously (Cao *et al.*, 2019). Knockout lines for *ZmCIPK12* were generated in the background of the B73-329 inbred line from the Center for

Crop Functional Genomics of China Agricultural University. Knockout lines for *ZmPPase4* were generated in the background of the B73-329 inbred line provided by WIMI Biotechnology (Jiangsu, China). Targeted mutations were detected by PCR amplifying the corresponding gene fragments and sequencing the PCR products. The edited plants were self-crossed, and homozygous plants were used for molecular and physiological analyses.

Transgenic maize construction

The coding sequence of *ZmCIPK12* was cloned into the *pCAMBIA3301* vector and transformed into *Agrobacterium* strain LBA4404 to infect immature embryos of the maize inbred line CAL. The transgene-positive plants of *ZmCIPK12* were backcrossed four times to maize inbred line B73 and then self-crossed until the BC_4F_8 generation. Physiological and molecular analyses were performed using the homozygous BC_4F_8 plants.

The sequence of *ZmCIPK12-HA* was cloned into the *pCAMBIA3301* vector, and the resulting construct was transformed into LBA4404 for subsequent infection of immature embryos from the maize inbred line Zong31.

The coding sequence of *ZmPPase4* was cloned into the *pCAMBIA3301-GFP* vector, and the resulting construct was transformed into LBA4404 for subsequent infection of immature embryos derived from the maize inbred line Zong31.

Yeast two-hybrid assay

ZmPPase4 coding region was cloned into the *pDEST22* vector to generate the *AD-ZmPPase4* construct, and the coding sequence of *ZmCIPK12* was cloned into the pDEST32 vector to generate *BD-ZmCIPK12*. The plasmids were cotransformed into the yeast strain MAV203 (ZC1615; Zymo Research, Irvine, CA, USA). Yeast dilution was spotted on selective mediums (SD/−Leu/−Trp with Agar, 630317 and SD/−Ade/–His/−Leu/−Trp with Agar, 630323; Clontech, Mountain View, CA, USA) and incubated for at least 3 d at 30°C before examining the yeast growth.

Measurement of Na^+ and K^+ contents

Maize samples of the shoot were dried at 80°C for 48 h and then treated in a muffle furnace at 300°C for 3 h and then 575°C for 6 h. The ashes were dissolved in 1% HCl, filtered through a 0.22-μm sterile syringe filter, and diluted with 1% HCl. Na^+ and K^+ contents in the solution were determined using the 4100-MP AES device (Agilent, Santa Clara, CA, USA).

GST pull-down assay

pGEX-4T-ZmCIPK12 and *pET30a-ZmPPase4* were each generated and transformed into *Escherichia coli* BL21(DE3). Glutathione S-transferase (GST)-tagged ZmCIPK12 protein was purified using glutathione agarose (16100; Thermo Scientific, Waltham, MA, USA), and His-tagged ZmPPase4 was purified using Ni-NTA agarose (30210; Qiagen). GST-ZmCIPK12 or GST coupled with the GST beads was incubated with ZmPPase4-His in the buffer solution (20 mM Tris–HCl, pH 7.5, 150 mM NaCl, 1 mM DTT (1,4-Dithiothreitol) and 1 mM PMSF (phenylmethanesulfonyl fluoride) at 4°C for 3 h with gentle shaking. The beads were washed five times with phosphate-buffered saline (PBS) buffer, followed by the addition of 6× sodium dodecyl sulfate (SDS) loading buffer and boiling for 5 min. Samples were detected by immunoblot assays using anti-His (D291-7; MBL ((Beijing) Biotech Co. Ltd, Beijing, China) and anti-GST (PM013-7; MBL) antibodies, respectively.

Co-immunoprecipitation assay

The co-immunoprecipitation (Co-IP) assays were performed in *Nicotiana benthamiana* leaves as described previously (Liu *et al.*, 2021) with minor modifications. Full-length *ZmCIPK12* and *ZmPPase4* coding sequences were inserted into the vectors *pCAMBIA1300-green fluorescent protein (GFP)* and *pCAMBIA1300-221-Flag*, respectively. Approximately 48 h after infiltration, 1 g of leaf tissue was used for protein extraction with lysis buffer (50 mM Tris–HCl, pH 7.5, 150 mM NaCl, 5 mM EDTA, pH 8.0, 0.1% Triton X-100, 0.2% NP-40, 0.6 mM PMSF, 20 μM MG132, and 1× protease inhibitor cocktail (04693124001; Roche)). Total proteins were incubated with anti-GFP mAb-Magnetic beads (D153-11; MBL) for 3 h at 4°C with rotation. After incubation, the magnetic beads were washed three times with lysis buffer. Then, protein loading buffer was added, and the samples were boiled at 100°C for 5 min. The antibodies used in this assay included anti-Flag (M185-7; MBL) and anti-GFP antibodies (598-7; MBL).

Split-luciferase assay

pCAMBIA-1300NLuc vector was digested with KpnI and SalI, and *pCAMBIA-1300CLuc* vector was digested by KpnI and BamHI. The coding sequences of *ZmCIPK12* and *ZmPPase4* were amplified and then cloned into *pCAMBIA-1300NLuc* and *pCAMBIA-1300CLuc*, respectively, using the pEASY®-Basic Seamless Cloning and Assembly Kit (CU201; TransGen Biotech, Beijing, China). These constructs were transferred into *Agrobacterium* strain GV3101 and infiltrated into *N. benthamiana* leaves. The infiltrated leaves were treated with 1 mM D-luciferin (E160E; Promega) for *c.* 5 min in the dark. Luminescent signals were detected using a plant imaging system (Tanon 5200, Tanon, Shanghai, China).

In vitro phosphorylation

Recombinant protein His-ZmPPase4 was incubated with GST-ZmCIPK12 and GST proteins in the reaction buffer (20 mM Tris–HCl, pH 7.5, 10 mM $MnCl_2$, 5 mM $CaCl_2$, 1 mM DTT, 10 mM ATP) at 30°C for 30 min. GST protein was used as a negative control. The reaction was stopped by adding 6 × SDS loading buffer. After boiling at 100°C for 5 min, phosphorylated proteins from the *in vitro* kinase assays were separated on 8% SDS-polyacrylamide gel electrophoresis (PAGE) gels containing 50 mM Phos-tag and detected using an anti-His antibody.

In vivo phosphorylation

One gram of leaf tissue was used for protein extraction with lysis buffer (50 mM Tris–HCl, pH 7.5, 150 mM NaCl, 0.1% Triton X-100, 0.2% NP-40, 0.6 mM PMSF, 20 μM MG132, 1× protease inhibitor cocktail, 1 mM ATP, and 1× PhosSTOP EASYpack (04906837001; Roche)). Total proteins were incubated with Anti-DDDDK-tag mAb-Magnetic Beads (M185-11R; MBL) at 4°C with rotation for 3 h. Following incubation, the magnetic beads were washed three times with lysis buffer. Half of the samples were supplemented with lambda protein phosphatase (λPP) and incubated at 30°C for 30 min. Subsequently, protein loading buffer was added, and the samples were boiled at 100°C for 5 min. Phosphorylated proteins were separated on 8% SDS-PAGE gels containing 50 mM Phos-tag and detected using an anti-Flag antibody.

Semi-*in vivo* kinase assay

Three grams of leaf tissue was used for protein extraction with lysis buffer identical to that employed in the *in vivo* phosphorylation assay. The total protein extract was incubated with Pierce Anti-HA Magnetic Beads (88836; Thermo Scientific) at 4°C overnight under constant rotation. After incubation, the beads were washed three times with PBS. Immunoprecipitated proteins on the magnetic beads were subsequently used for the *in vitro* phosphorylation assay. Antibodies used for immunoprecipitation included anti-His and anti-HA (M180-7; MBL).

Cell-free protein degradation assay

Cell-free protein degradation assays were performed as described previously (Ma *et al.*, 2021) with minor modifications. Maize seedlings were treated with or without 200 mM NaCl for 24 h after growing normally for 8 d. Two hundred nanograms of purified recombinant His-ZmPPase4 protein was added to cell-free extracts, with or without the addition of 50 μM MG132, and incubated at 25°C for the indicated times. The reactions were stopped by the addition of 6 × SDS sample buffer. The proteins were subsequently separated by 12% SDS-PAGE and detected with anti-His and anti-actin antibodies (ET1701-80; HuaBio, Hangzhou, Zhejiang, China).

Transmission electron microscopy

Maize leaves were sectioned transversely into pieces with a width ranging from 1 to 2 mm, followed by fixation in a 2.5% glutaraldehyde solution. The sectioned leaves were then rinsed with 0.1 M phosphate buffer and dehydrated through a gradient of ethanol solutions, followed by pure acetone. The samples were then subjected to a 1 : 1 and 1 : 3 mixture of resin and acetone, after which they were immersed in pure resin for polymerization. Ultrathin sections were observed using a transmission electron microscope (HT7700; Hitachi Co. Ltd, Tokyo, Japan).

Results

ZmCIPK12 positively regulates salt tolerance in maize seedlings

In order to identify CIPKs' function in salt stress responses, we analyzed the expression of *CIPK* genes in maize seedlings in response to a 24-h NaCl treatment from RNA sequencing data. A few *CIPK* genes exhibited significant expression induction by salt, *Zm00001eb292760*, named as *ZmCIPK12* (Zhou *et al.*, 2022), having the highest induction by salt treatment (Fig. 1a; Table S2).

To analyze the function of *ZmCIPK12* in salt tolerance, we obtained two CRISPR/Cas9 edited mutants, *zmcipk12-1* and *zmcipk12-2*, in the B73-329 background. The *zmcipk12-1* mutant harbored a 1-bp insertion, and the *zmcipk12-2* mutant harbored a 5-bp deletion (Fig. 1b), both leading to frameshifts in the coding region. Under normal growth conditions, the two *ZmCIPK12* mutant lines did not have a morphological difference compared with the B73-329 wild-type ($WT^{B73\text{-}329}$). However, after 200 mM NaCl treatment for 2 wk, the *zmcipk12-1* and *zmcipk12-2* seedlings appeared more withered than the $WT^{B73\text{-}329}$ (Fig. 1c). The *zmcipk12-1* and *zmcipk12-2* plants also had lower fresh and dry weights of shoots than the $WT^{B73\text{-}329}$ after NaCl treatment (Fig. 1d,e). The Na^+ content and the Na^+ : K^+ ratio in shoots were significantly higher in the mutants than in the $WT^{B73\text{-}329}$, while there was no significant difference in K^+ content between the mutants and the $WT^{B73\text{-}329}$ (Fig. 1f–h). These results indicate that the loss of *ZmCIPK12* function causes salt susceptibility in maize seedlings.

We further determined whether or not *ZmCIPK12* OE enhances salt tolerance in maize. *ZmCIPK12* was expressed under the control of the 35S promoter in the maize B73 background. The transcript level of *ZmCIPK12* was higher in the OE lines, OE1 and OE2, than in the B73 wild-type (WT^{B73}) as detected by qRT-PCR (Fig. 1i). *ZmCIPK12* OE lines and WT^{B73} plants had no obvious detectable differences under nonstress conditions. After a 200 mM NaCl salt treatment, OE1 and OE2 plants were significantly more robust and had higher fresh weight and dry weight of shoots than the WT^{B73} (Fig. 1j–l). They also had lower Na^+ content, higher K^+ content, and lower Na^+ : K^+ ratio under salt treatment compared with the WT^{B73} (Fig. 1m–o). Together, these observations indicate that *ZmCIPK12* positively regulates the salt tolerance of maize seedlings.

ZmCIPK12 interacts with a soluble inorganic pyrophosphatase

We found that ZmCIPK12 is likely a canonical CIPK because it interacts with CBL proteins ZmCBL4 and ZmCBL8 (Zhang *et al.*, 2016) as shown by the yeast two-hybrid assay (Y2H) and bimolecular fluorescence complementation (BiFC; Fig. S1a,b).

To investigate how ZmCIPK12 protein regulates salt tolerance, *ZmCIPK12* was constructed into the *pDEST32* vector and used as a bait to screen a yeast library, resulting in the acquisition of 36 yeast clones. Through PCR detection, sequencing, and

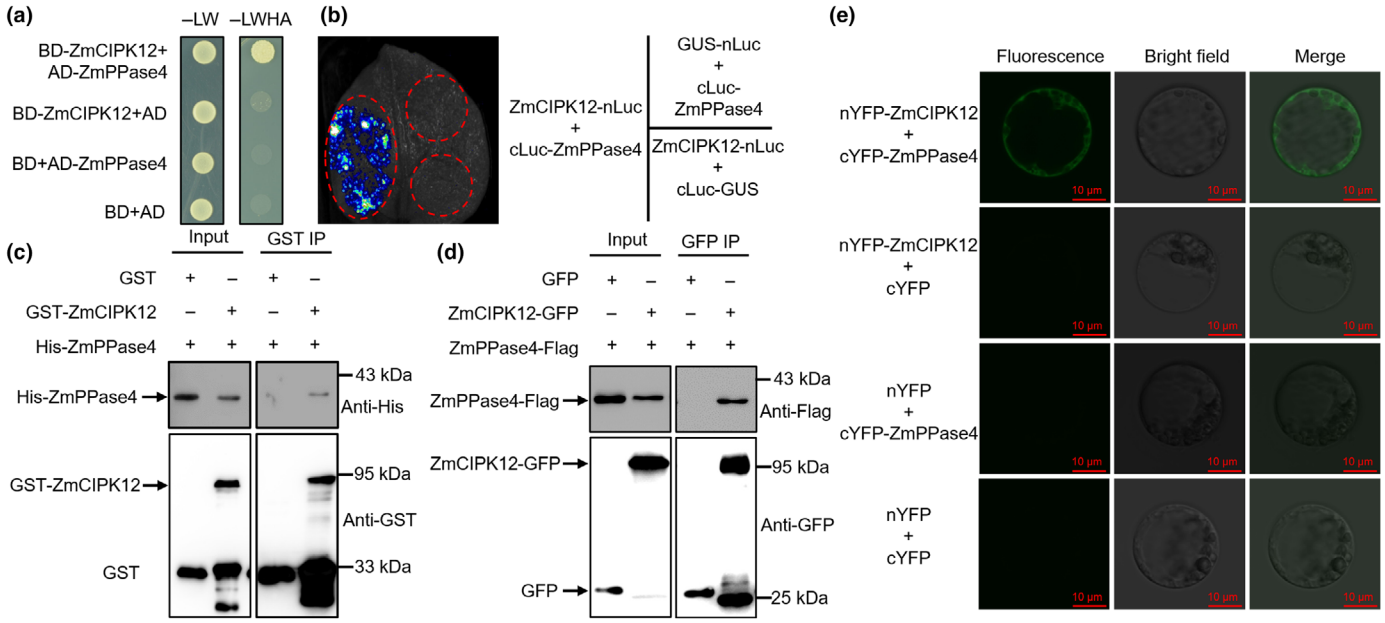

Fig. 2 ZmCIPK12 interacts with ZmPPase4. (a) ZmCIPK12 interacts with ZmPPase4 in a yeast two-hybrid assay. Yeast cells were cotransformed with BD-ZmCIPK12 and AD-ZmPPase4 constructs and plated on −Leu/−Trp (−LW) and −Leu/−Trp/−His/−Ade (−LWHA) with 15 mM 3AT (3-amino-1,2,4-triazole) medium. (b) Split-luciferase assay was performed to test the interaction between ZmCIPK12 and ZmPPase4. ZmCIPK12-nLUC and cLuc-ZmPPase4 were co-injected into *Nicotiana benthamiana* leaves. ZmCIPK12-nLuc/cLuc-GUS and GUS-nLuc/cLuc-ZmPPase4 were used as negative controls. The luminescence signals were detected using a CCD (charge-coupled device) camera. (c) GST pull-down assay showing the interaction between GST-ZmCIPK12 and His-ZmPPase4. GST-ZmCIPK12 and His-ZmPPase4 were purified from BL21(DE3). GST-ZmCIPK12 and GST were detected by an anti-GST antibody. His-ZmPPase4 was detected by an anti-His antibody. GST served as a negative control. (d) Co-immunoprecipitation assay showing the *in vivo* interaction between ZmCIPK12 and ZmPPase4. ZmCIPK12-GFP or GFP was co-injected with ZmPPase4-Flag into *N. benthamiana* leaves. Total protein extracts were immunoprecipitated with anti-GFP magnetic beads. Immunoblotting was detected with anti-GFP and anti-Flag antibodies. (e) Bimolecular fluorescence complementation experiments confirm the interaction in maize protoplasts. Full-length ZmCIPK12 was fused to nYFP (the N-terminal part of YFP), and ZmPPase4 was fused to cYFP (the C-terminal part of YFP). Bars, 10 μm. IP, immunoprecipitation.

Y2H, we identified five interacting proteins. In this screen, ZmPPase4 coded by *Zm00001eb266490* (Z. Chen *et al.*, 2021) was identified as a ZmCIPK12-interacting partner. ZmPPase4 is in the soluble pyrophosphatase family and is highly homologous to the Arabidopsis AtPPase4 and rice OsPPase4 (Fig. S2).

The Y2H assay was used to confirm the interaction between ZmCIPK12 and ZmPPase4 by reconstructing full-length proteins. The yeast strains cotransformed with *AD-ZmPPase4* and -*BD-ZmCIPK12* grew well on the selective medium (SD/−Trp/−Leu/−His/−Ade). By contrast, the yeast strains cotransformed with *BD-ZmCIPK12* and AD, *AD-ZmPPase4* and BD, as well as AD and BD, all failed to grow on the selective medium (Fig. 2a). The interaction between ZmCIPK12 and ZmPPase4 was further validated using a split-luciferase assay. Co-expression of nLuc-ZmCIPK12 and cLuc-ZmPPase4 in *N. benthamiana* produced a strong luminescence signal at 48 h, while the control pairs did not generate any signal (Fig. 2b). The interaction between ZmCIPK12 and ZmPPase4 was direct, as shown by a GST pull-down assay. Recombinant GST-ZmCIPK12 protein, rather than GST, specifically pulled down the recombinant His-ZmPPase4 protein (Fig. 2c). The interaction between these two proteins was further supported by an *in planta* Co-IP assay. When expressed in *N. benthamiana* leaves, ZmCIPK12-GFP, but not GFP, was able to precipitate its co-expressed ZmPPase4-Flag (Fig. 2d). The BiFC assay also confirmed the interaction between ZmCIPK12 and ZmPPase4 in the cytoplasm of maize protoplasts (Fig. 2e). This is further supported by the similar cytosol and plasma membrane localizations in cells of ZmCIPK12 and ZmPPase4, which were examined by their yellow fluorescent protein (YFP) fusions transiently expressed in *N. benthamiana* leaves. Both ZmCIPK12-YFP and ZmPPase4-YFP were localized to the cytoplasm and the plasma membrane (Fig. S3), further supporting their interaction in plants. Taken together, these results indicate that ZmCIPK12 interacts with ZmPPase4 both *in vitro* and *in vivo*.

ZmCIPK12 enhances ZmPPase4 protein stability through phosphorylation

Because CIPKs are Ser/Thr protein kinases (Fu *et al.*, 2023), we investigated whether or not ZmCIPK12 phosphorylates ZmPPase4. The GST-ZmCIPK12 protein was co-incubated with the His-ZmPPase4 protein and subjected to Phos-tag SDS-PAGE. In the presence of GST-ZmCIPK12, a shifted band of His-ZmPPase4 was detected using an anti-His antibody, suggesting that ZmCIPK12 phosphorylates ZmPPase4 *in vitro* (Fig. 3a). To identify the phosphorylation sites in ZmPPase4 by ZmCIPK12, we utilized liquid chromatography tandem mass

spectrometry (LC-MS/MS) analysis to detect phosphorylation sites of ZmPPase4 in the presence of ZmCIPK12. Serine-191 (S191) in ZmPPase4 was identified as a potential site phosphorylated by ZmCIPK12 (Fig. S4). We mutated S191 to Ala (A) to generate the nonphosphorylated form of His-ZmPPase4^{S191A} for Phos-tag mobility shift assay. The shifted band observed in the WT ZmPPase4 was not observed for ZmPPase4^{S191A}, indicating that the S191 is the major site phosphorylated by ZmCIPK12 (Fig. 3a). We transiently expressed ZmPPase4-Flag along with GFP or ZmCIPK12-GFP in *N. benthamiana* leaves. In the presence of ZmCIPK12-GFP, Phos-tag gel analysis revealed a slightly enhanced signal for the shifted band corresponding to phosphorylated ZmPPase4-Flag. Furthermore, these shifted bands disappeared after treatment with λPP (Fig. S5a). These results indicate that ZmCIPK12 may phosphorylate ZmPPase4 *in vivo*.

We treated 2-wk-old ubi:ZmCIPK12-HA maize seedlings with 200 mM NaCl. ZmCIPK12-HA protein was immunoprecipitated from transgenic maize seedlings with or without salt treatment using anti-HA magnetic beads, and *in vitro* phosphorylation assays were performed with His-ZmPPase4 as substrate. Compared with 0 h, the intensity of the shifted band increased in samples from the 5-h salt treatment, whereas no shifted band was detected in Phos-tag gels in the absence of ZmCIPK12-HA (Fig. 3b). These results may suggest that the kinase activity of ZmCIPK12 is induced by NaCl treatment.

Phos-tag gel assays were also performed to detect the phosphorylation of ZmPPase4. Total proteins were extracted from maize seedlings of the ubi:ZmPPase4-GFP OE line at the indicated time points following salt treatment. The shifted band of ZmPPase4-GFP was detected at 0 h, and the intensity of the shifted band increased at 3 h. When total proteins were treated with λPP, the phosphorylated forms of ZmPPase4 observed at 12 h were nearly eliminated (Fig. S5b). These results indicate that NaCl treatment may induce phosphorylation of ZmPPase4 *in vivo*.

To determine the biological significance of ZmPPase4 phosphorylation by ZmCIPK12, we performed cell-free degradation assays using extracts from maize seedlings on both phosphorylation defective mutant ZmPPase4^{S191A} and phosphorylation mimic mutant ZmPPase4^{S191D}. His-tagged fusion proteins were incubated in cell extracts from WT^{B73} seedlings in the presence of ATP, and the samples were collected at various points of incubation for protein blot analysis. The His-ZmPPase4^{S191A} mutant protein was degraded markedly faster than the WT His-ZmPPase4. By contrast, the His-ZmPPase4^{S191D} was degraded more slowly than His-ZmPPase4 (Fig. 3c). The recombinant His-ZmPPase4 protein was also incubated in cell extracts from the *zmcipk12-1* mutant. The WT His-ZmPPase4 protein was degraded more quickly in *zmcipk12-1* extracts than in the WT$^{B73\text{-}329}$ extracts (Fig. 3d). In the *zmcipk12-1* extracts, the degradation rate of His-ZmPPase4^{S191A} protein was comparable to that of the WT His-ZmPPase4, while the His-ZmPPase4^{S191D} degraded more slowly than the WT His-ZmPPase4 (Fig. 3e). When the proteasome inhibitor MG132 was added, the degradation rates of His-ZmPPase4, His-ZmPPase4^{S191A}, and His-ZmPPase4^{S191D} in both WT$^{B73\text{-}329}$ and *zmcipk12-1* extracts were all greatly reduced (Fig. 3f,g).

We further measured the content of all pyrophosphatases in WT$^{B73\text{-}329}$ and the *zmcipk12* mutant plants by enzyme-linked immunosorbent assay. Under normal treatment, no difference in the content of PPase was observed between the *zmcipk12* mutants and the WT$^{B73\text{-}329}$ plants. By contrast, PPase content was significantly lower in *zmcipk12-1* and *zmcipk12-2* plants than in WT$^{B73\text{-}329}$ under salt treatment (Fig. 3h). The two *ZmCIPK12* OE lines did not exhibit a difference in the content of PPase from WT^{B73} under control conditions, but displayed a higher content of PPase than the WT^{B73} under salt treatment (Fig. 3i). These results indicate that accumulation of total PPase proteins is enhanced by ZmCIPK12, which is consistent with the notion that the stability of the ZmPPase4 protein is enhanced by ZmCIPK12.

The loss of ZmPPase4 function reduces salt tolerance

To investigate whether ZmPPase4 is a mediator of ZmCIPK12 function, we examined the function of ZmPPase4 in salt tolerance. The expression of *ZmPPase4* was significantly induced by salt stress at 4 h after 100 mM NaCl salt treatment as determined by qRT-PCR (Fig. S6). We used the CRISPR/Cas9 system for gene editing and generated two loss of function *ZmPPase4* alleles with a 404-bp deletion and a 605-bp deletion in the *ZmPPase4* gene (Fig. 4a). The homozygous *zmppase4* mutant plants were selected and confirmed by agarose gel electrophoresis of PCR products at the edited region (Fig. 4b). Under regular growth conditions, *zmppase4-1* and *zmppase4-2* mutants grew similarly to the WT. However, when exposed to 200 mM NaCl, *zmppase4-1* and *zmppase4-2* plants had yellower and curlier leaves compared with WT$^{B73\text{-}329}$, exhibiting a salt-susceptible phenotype (Fig. 4c). The *zmppase4-1* and *zmppase4-2* mutants also exhibited decreased fresh weight and dry weight compared with the WT$^{B73\text{-}329}$ under high salinity conditions but not under nonstress conditions (Fig. 4d,e). When treated with salt, the *zmppase4* seedlings displayed a higher Na^+ accumulation but not a higher K^+ level than the WT$^{B73\text{-}329}$ (Fig. 4f,g). The differential Na^+ content was also reflected by the Na^+ : K^+ ratio, which was higher in *zmppase4* mutant plants than in the WT$^{B73\text{-}329}$ (Fig. 4h). Taken together, these results suggest that *ZmPPase4* also has a role in salt stress tolerance.

ZmCIPK12 and ZmPPase4 affect cell wall thickness under salt stress

Because Arabidopsis PPases was implicated in cell wall modulation and the cell wall is implicated in salt tolerance (Segami *et al.*, 2018; Dabravolski & Isayenkov, 2023), we explored whether ZmCIPK12 and ZmPPase4 might regulate the cell wall for salt tolerance. We imaged and quantified cell wall thickness of sclerenchyma in the 3rd leaf of plants by TEM. Each mutant in different backgrounds was compared with its corresponding WT. When seedlings were treated with 200 mM NaCl, the sclerenchyma cell wall had markedly thinner cell walls in

zmppase4 plants than in the WT$^{B73-329}$ under saline conditions, while no significant difference was observed under nonstress conditions (Fig. 5a–g). In addition, the cell wall was thinner in *zmcipk12-1* and *zmcipk12-2* mutant seedlings than in the WT$^{B73-329}$ plants, while no significant difference was apparent under control conditions (Fig. 5h–n). Furthermore, the

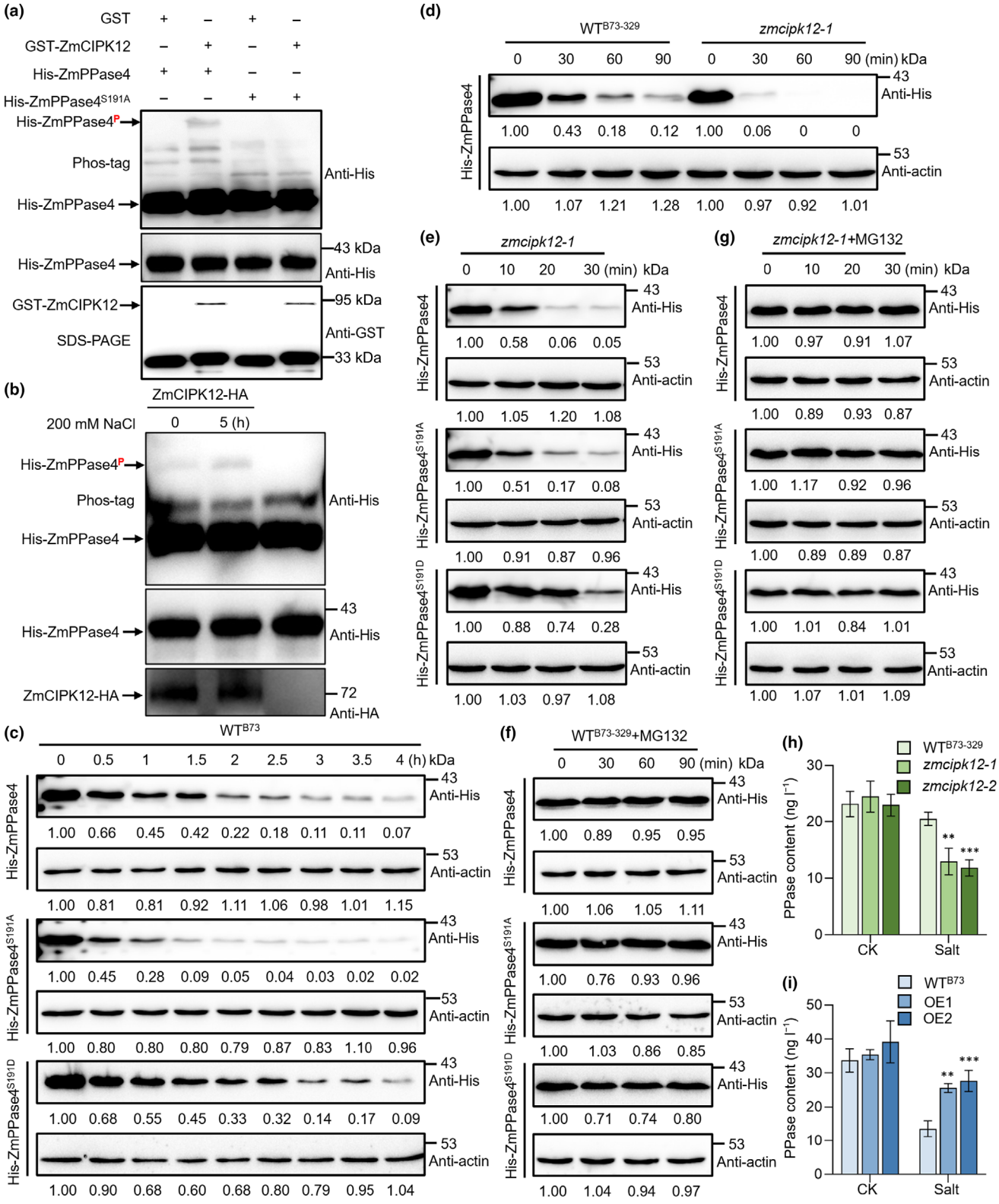

Fig. 3 ZmCIPK12 phosphorylates and stabilizes ZmPPase4. (a) ZmCIPK12 phosphorylates ZmPPase4 *in vitro*. Recombinant His-ZmPPase4 or His-ZmPPase4^{S191A} was incubated with GST-ZmCIPK12 in kinase buffer and then analyzed by Phos-tag mobility shift assay. (b) Kinase activity of ZmCIPK12 on ZmPPase4. Maize seedlings were treated with 200 mM NaCl. ZmCIPK12-HA was immunoprecipitated and incubated with recombinant His-ZmPPase4 proteins for an *in vitro* kinase assay. The proteins were detected with anti-HA and anti-His antibodies by immunoblotting. (c) Cell-free degradation assays show that His-ZmPPase4^{S191D} protein is degraded more slowly than both His-ZmPPase4 and His-ZmPPase4^{S191A} in WT^{B73} extracts. Total protein extracts were isolated from 8-d-old leaves of B73. The abundance of recombinant protein was analyzed by immunoblotting using an anti-His antibody. Actin was used as a loading control, and the relative protein levels were quantified using the ImageJ software. (d) The stability of His-ZmPPase4 protein in the WT$^{B73\text{-}329}$ and *zmcipk12-1* extracts. (e) Cell-free degradation assays show that His-ZmPPase4^{S191D} protein is degraded more slowly than His-ZmPPase4 and His-ZmPPase4^{S191A} in *zmcipk12-1* extracts. (f, g) The degradation patterns of His-ZmPPase4, His-ZmPPase4^{S191A}, and His-ZmPPase4^{S191D} were analyzed in the WT$^{B73\text{-}329}$ (f) and *zmcipk12-1* (g) extracts with MG132 (proteasome inhibitor). (h) Total PPase content of WT$^{B73\text{-}329}$, *zmcipk12-1*, and *zmcipk12-2* under normal and salt treatment conditions. Total proteins were extracted from the third leaves of plants and detected using a Plant PPase ELISA Kit. (i) Total PPase content of WT^{B73} and *ZmCIPK12* overexpression lines in normal and salt treatment conditions. Error bars show the mean ± SD (n = 3). Statistical significance was determined by a two-way ANOVA: **, $P < 0.01$; ***, $P < 0.001$. P, phosphorylation; WT, wild-type.

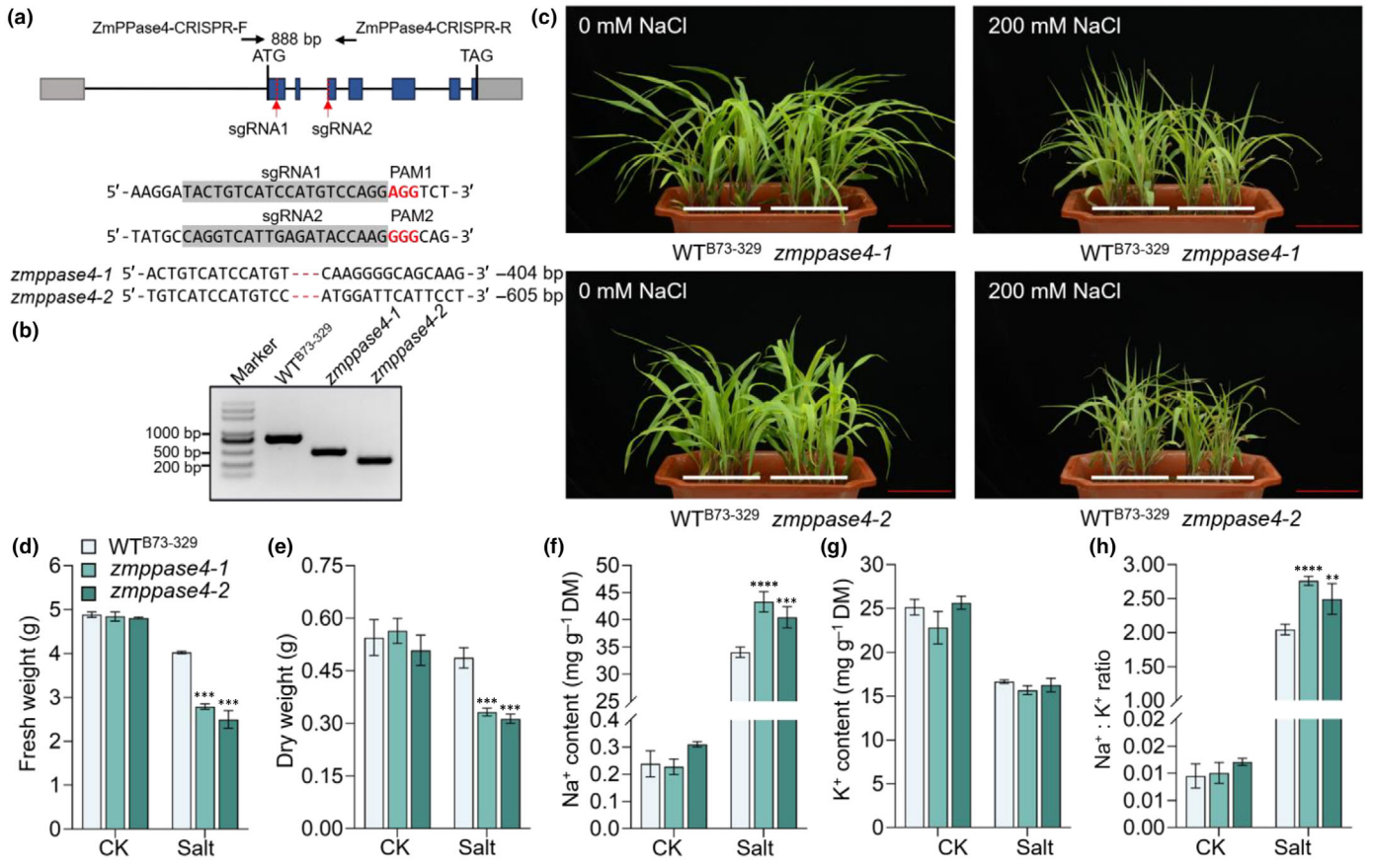

Fig. 4 Phenotype of *zmppase4* mutants under normal and salt stress conditions. (a) Two homozygous CRISPR/Cas9 knockout lines with deletions in the target site of *ZmPPase4*. The gene model and wild-type (WT) sequence are shown at the upper panel. Protospacer adjacent motif (PAM) sequences are highlighted in red. Red arrows indicate the target sites in *ZmPPase4*. Black arrows indicate the primers used to detect the *zmppase4* mutants. (b) Results of PCR amplifications for WT$^{B73\text{-}329}$, *zmppase4-1*, and *zmppase4-2* plants. (c) Phenotypic comparison of WT$^{B73\text{-}329}$, *zmppase4-1*, and *zmppase4-2* plants grown under control and salt stress conditions. (d–h) Comparison of shoot fresh weight (d), dry weight (e), Na^+ content (f), K^+ content (g), and Na^+ : K^+ ratio (h) between WT$^{B73\text{-}329}$ and *zmppase4* plants under normal and salt treatment conditions. Three seedlings were collected for the assessment of indicators. Bars, 10 cm. Error bars show the mean ± SD (n = 3). Statistical significance was determined by a two-way ANOVA: **, $P < 0.01$; ***, $P < 0.001$; ****, $P < 0.0001$. CK, control check.

sclerenchyma cells in *ZmCIPK12* OE plants (OE1 and OE2) were markedly thicker than those in the WT^{B73} under salt treatment but not under nonstress conditions (Fig. 5o–u). These results indicate that ZmCIPK12 and ZmPPase4 both affect cell wall thickness under salt stress.

ZmCIPK12 and *ZmPPase4* affect the expression of cell wall-related genes

We analyzed the transcriptome profiles of WT$^{B73\text{-}329}$ and *zmcipk12-1* with and without a 24-h salt stress to further explore

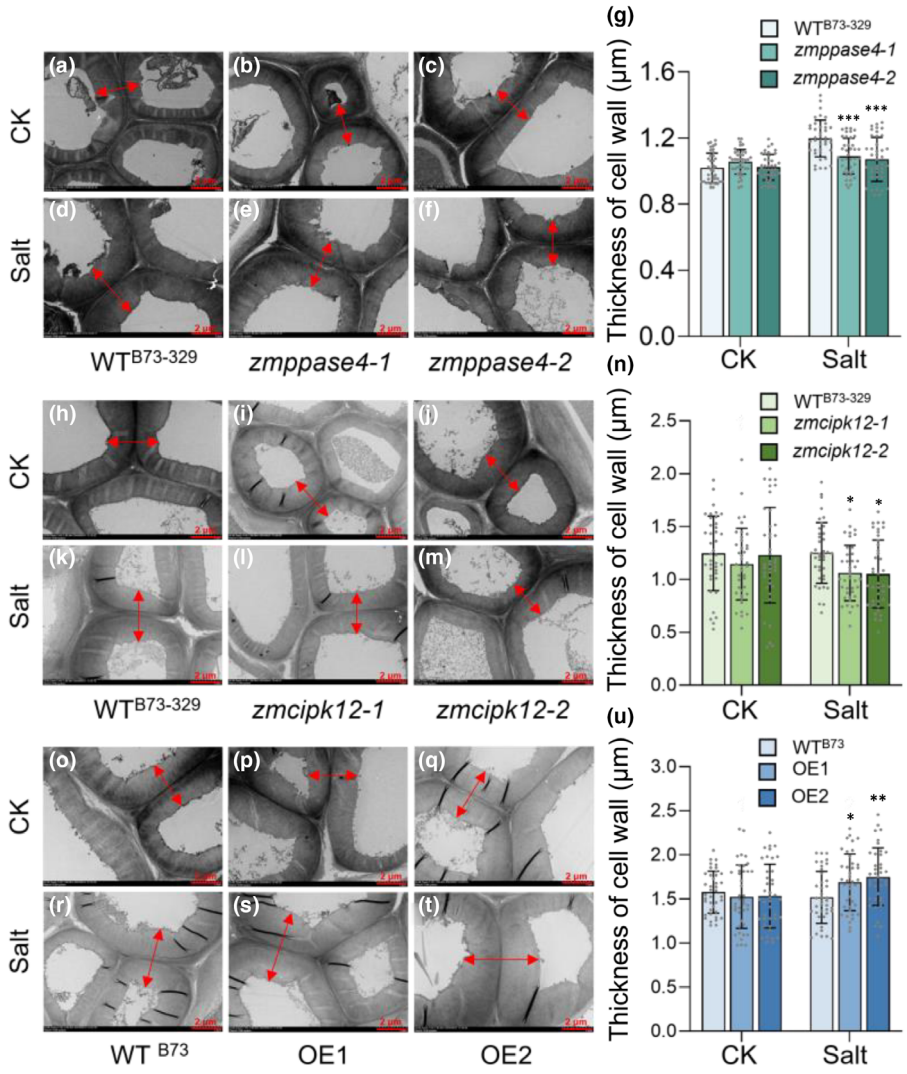

Fig. 5 ZmPPase4 and ZmCIPK12 affect the thickness of sclerenchyma cell walls in leaves. (a–f) Transmission electron microscopy (TEM) images of sclerenchyma cell walls of $WT^{B73-329}$, *zmppase4-1*, and *zmppase4-2* under normal and salt stress conditions. The $WT^{B73-329}$ and *zmppase4* mutants were provided by WIMI Biotechnology (Jiangsu, China). Seedlings (8 d old) were treated with or without a 200 mM NaCl treatment for 5 d. (g) Statistical analysis of sclerenchyma cell wall thickness in $WT^{B73-329}$ and *zmppase4* plants. (h–m) TEM images of sclerenchyma cell walls of $WT^{B73-329}$, *zmcipk12-1*, and *zmcipk12-2* under normal and salt stress conditions. The $WT^{B73-329}$ and *zmcipk12* mutants with a B73-329 background were provided by the Center for Crop Functional Genomics of China Agricultural University. (n) Statistical analysis of sclerenchyma cell wall thickness in $WT^{B73-329}$ and *zmcipk12* plants. (o–t) TEM images of sclerenchyma cell walls of WT^{B73} and *ZmCIPK12* overexpression lines under normal and salt stress conditions. *ZmCIPK12* transgenic materials were constructed with a B73 background. (u) Statistical analysis of sclerenchyma cell wall thickness in WT^{B73} and *ZmCIPK12* overexpression plants. Bars, 2 μm. Error bars show the mean ± SD (n = 40). Statistical significance was determined by a two-way ANOVA: *, $P < 0.05$; **, $P < 0.01$; ***, $P < 0.001$. CK, control check; OE, overexpression; WT, wild-type.

the potential mechanisms underlying the role of *ZmCIPK12* in salt tolerance. Based on the criteria of the twofold expression change and false discovery rate < 0.05, 305 DEGs were identified between *zmcipk12-1* and $WT^{B73-329}$ plants under normal conditions (Table S3), and 993 DEGs were identified between *zmcipk12-1* and $WT^{B73-329}$ plants under salt conditions (Table S4). A total of 914 DEGs were specifically induced after salt treatment in *zmcipk12-1*, among which 382 DEGs were upregulated (Table S5) and 532 DEGs were downregulated (Fig. 6a; Table S6). Gene Ontology (GO) analysis revealed that the 382 upregulated genes were enriched mostly in terms such as 'response to organic substance', 'response to endogenous stimulus', and 'response to water deprivation' (Fig. 6b). Five hundred and thirty-two downregulated genes were enriched in terms such as 'ion binding', 'extracellular region', and 'response to endogenous stimulus' (Fig. 6c). Interestingly, some of the salt downregulated genes in the mutant have known or presumed functions associated with the cell wall, including 4-coumarate-CoA ligase 16 (*Zm4CL16*, *Zm00001eb187910*), flavone synthase 1 (*ZmFNS1*, *Zm00001eb394430*), red aleurone 1 (*ZmPR1*, *Zm00001eb245960*), phenylalanine ammonia-lyase 7 (*ZmPAL7*, *Zm00001eb247660*), *ZmCYP73A8* (*Zm00001eb240910*), pectin methylesterase 19 (*ZmPME19*, *Zm00001eb130500*), peroxidase 61 (*ZmPRX61*, *Zm00001eb330540*), and *ZmPRX78* (*Zm00001eb330550*). qRT-PCR experiments demonstrated that under salt treatment, the relative expression levels of these genes in the mutants were significantly downregulated compared with the $WT^{B73-329}$ (Fig. S7a–h). Given that some of these genes may be involved in lignin biosynthesis, we assayed lignin content in the *zmcipk12* mutant and found that it was indeed reduced under salt stress (Fig. S8).

We further analyzed the transcriptome profiles of $WT^{B73-329}$ and *zmppase4-2* plants under both 24-h salt stress and nonstress conditions. Under normal conditions, 528 DEGs were identified by the comparison between $WT^{B73-329}$ and *zmppase4-2* (Table S7). Five hundred and twelve DEGs were identified between $WT^{B73-329}$ and *zmppase4-2* plants under salt conditions (Table S8). A total of 462 DEGs were specifically regulated in *zmppase4-2*, consisting of 114 upregulated (Table S9) and 348 downregulated genes (Fig. S9a; Table S10). GO analysis revealed

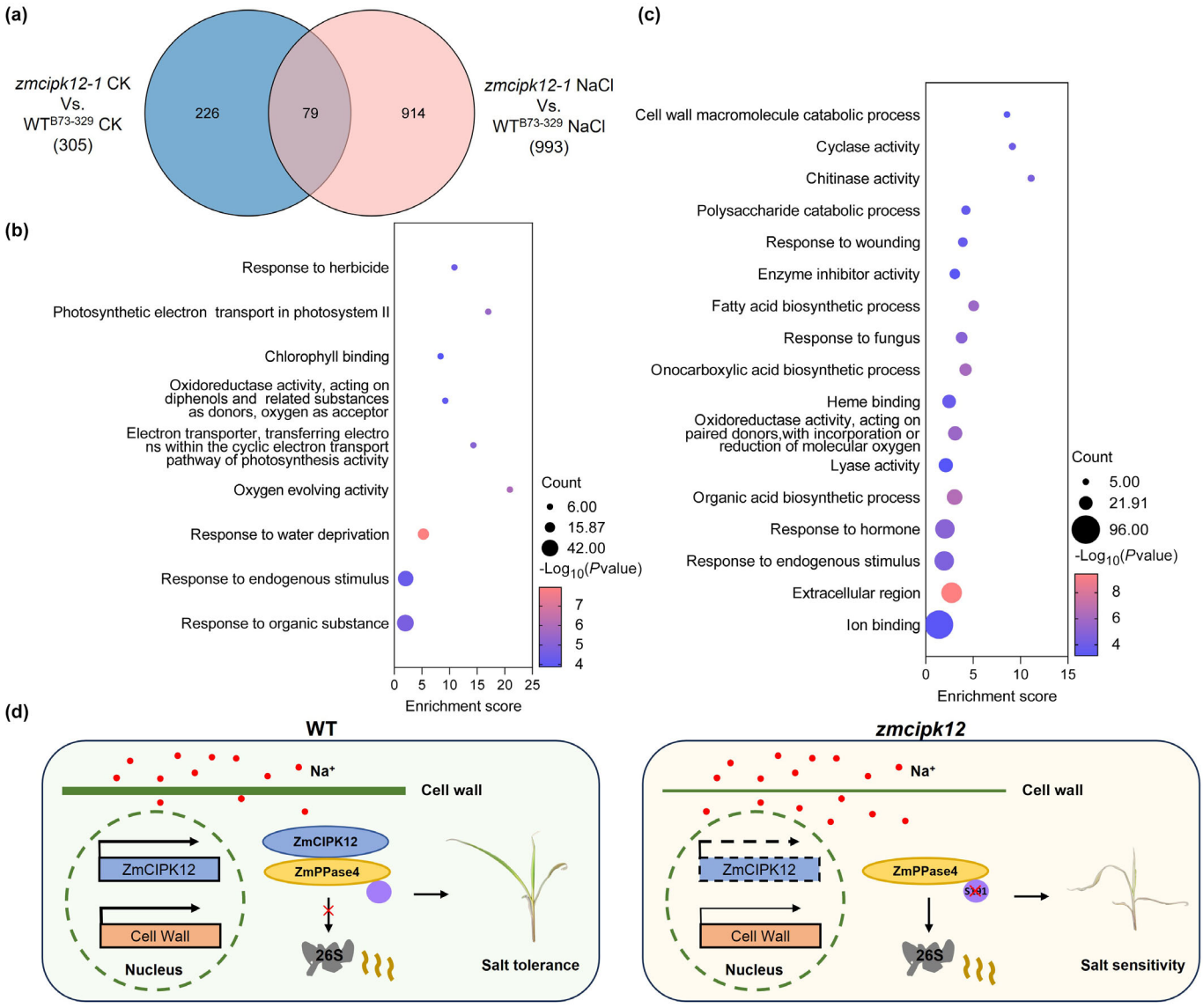

Fig. 6 Transcriptomic analysis of *ZmCIPK12*-regulated salt-responsive genes. (a) The Venn diagram shows the number of genes between WT$^{B73\text{-}329}$ and *zmcipk12-1* under both normal and saline conditions. (b) Gene Ontology (GO) analysis of the 382 differentially expressed genes (DEGs) specifically upregulated in *zmcipk12-1*. The color code represents the $\log_{10}$(*P*-value) at the right of the panel. (c) GO analysis of the 532 DEGs specifically downregulated in *zmcipk12-1*. (d) Working model of *ZmCIPK12* regulating salt tolerance in maize. In wild-type (WT) plants, high Na^+ levels trigger the transcriptional upregulation of *ZmCIPK12*. The ZmCIPK12 protein subsequently phosphorylates ZmPPase4, thereby inhibiting the degradation of ZmPPase4 by the 26S proteasome. ZmCIPK12 stabilizes ZmPPase4 and affects the expression of cell wall-related genes, by both thickening the cell wall and promoting salt tolerance in maize. Conversely, in *zmcipk12* plants, the loss of ZmCIPK12 function results in decreased transcript levels of the cell wall-related genes and degradation of ZmPPase4, which leads to a thinner cell wall and increased sensitivity to salt stress. Cell walls and nuclei are denoted by green solid and dashed lines, respectively. Transcriptional and non-transcriptional expression are represented by long solid and long dashed arrows, respectively.

that the 114 upregulated genes were exclusively enriched in the 'extracellular region' term. The 348 downregulated genes were enriched in terms including 'cell periphery', 'defense response', and 'response to salt stress' (Fig. S9b). Additionally, qRT-PCR analysis demonstrated that the expression levels of several cell wall-related genes were reduced in the *zmppase4* mutants under salt stress, including UDP-glucose transporter 2 (*ZmUTR2*, *Zm00001eb403950*), *ZmPRX61*, *ZmPRX71* (*Zm00001eb276250*), Caffeic acid O-methyltransferase 25 (*ZmCOMT25*, *Zm00001eb400190*), *ZmPAL7* and *ZmPME41* (*Zm00001eb327190*) (Fig. S10a–f). Some cell wall-related genes were downregulated in both the *zmcipk12* and *zmppase4* mutants, such as *ZmPAL7* and *ZmPRX61* (Figs S7d,g, S10c,e). These results suggest that *ZmCIPK12* and *ZmPPase4* may cooperatively or independently affect cell wall-related genes.

Discussion

Although previous studies have suggested a key role for CIPKs-mediated salt signaling in plants (Ali *et al.*, 2023), the

mechanisms by which and how *CIPKs* regulate salt tolerance in maize remain largely elusive. Here, we have shown that a CIPK family gene, *ZmCIPK12*, contributes to salt tolerance in maize (Fig. 1a–o). ZmCIPK12 phosphorylates ZmPPase4 at Ser191 and enhances its protein stability (Fig. 3a,c–g). Few *sPPase* genes have been found to affect salt tolerance in plants. We show that the loss of ZmPPase4 function causes maize to be sensitive to salt stress (Fig. 4a–h). Moreover, ZmCIPK12 and ZmPPase4 positively affect cell wall thickness under salt stress (Fig. 5a–u).

Plants have developed various strategies to adapt to salt stress (Zhao *et al.*, 2021). One strategy is the well-studied SOS pathway that facilitates Na^+ exclusion and compartmentalization to enhance salt tolerance (Zhou *et al.*, 2022; Ramakrishna *et al.*, 2025). This study identifies a new player, *ZmCIPK12*, in salt tolerance in maize, which might function in a process different from the SOS pathway (Fig. 6d). The stress signal is thought to be detected by cell wall sensors on the plasma membrane, which triggers a cascade of downstream responses (Zhao *et al.*, 2021). ZmCIPK12 could play a role in transmitting stress signals to ZmPPase4 through phosphorylation, thereby influencing the cell wall under saline conditions.

The sPPases can be phosphorylated at different amino acid residues, and their phosphorylation has a variety of functions in plant cells. Calcium-dependent protein kinases (CPKs) are shown to phosphorylate sPPases at their N-terminal extensions (Eaves *et al.*, 2017). ZmCIPK12 catalyzes the phosphorylation at S191, which is located in the C terminus of ZmPPase4 (Figs 3a, S2). These studies suggest that different stimuli may cause phosphorylation of sPPase at distinct sites in plants. Previous studies also have identified phosphorylation regulation of sPPase proteins. Phosphorylation of an sPPase in pollen tubes inhibits its activity (De Graaf *et al.*, 2006). Phosphorylation is often coupled with ubiquitination to alter the protein stability in plants (Liu *et al.*, 2023; Ma *et al.*, 2023). We propose that ZmCIPK12 promotes the accumulation of ZmPPase4 through phosphorylation-induced protein stability. The degradation rate of His-ZmPPase4^{S191A} protein is much quicker than the WT His-ZmPPase4 (Fig. 3c). The total amount of PPase proteins reduced in the *zmcipk12* mutant is shown in Fig. 3(h,i), suggesting that ZmCIPK12 might regulate other PPases in addition to ZmPPase4.

CIPKs have been implicated in cell wall regulation. OE of *PdCIPK21* or *PdCIPK31* enhances Arabidopsis salt tolerance and increases cell wall thickness in the Arabidopsis stem regardless of salt stress (Chen *et al.*, 2025). Here, ZmCIPK12 is shown to affect the cell wall of maize under salt stress (Fig. 5h–u). Downregulated cell wall genes in *zmcipk12* and *zmppase4* mutants suggest they may cooperatively or independently affect cell wall-related genes (Figs S7, S10). However, it remains unclear how ZmCIPK12 and its target protein ZmPPase4 regulate the cell wall, and the mechanism may be further elucidated using the *zmcipk12/zmppase4* double mutants in the future.

The structure and composition of the cell wall are associated with the salt tolerance of plants (Dabravolski & Isayenkov, 2023). ZmCIPK12 and ZmPPase4 both affect cell wall thickness under salt stress (Fig. 5a–u), suggesting their regulation of the cell wall for salt tolerance or a strong association of salt tolerance with cell wall modification. The association has been observed in a prior study of a maize laccase gene. OE of a laccase increased lignin deposition, thickened the cell wall and increased salt tolerance in maize (Qin *et al.*, 2023). Our findings point to a salt-dependent influence of cell wall thickness by ZmCIPK12 and ZmPPase4. The susceptibility of mutants to salt may result from a reduced physical barrier defense. Cell walls support cell growth and act as a physical barrier to protect cells from environmental changes (Colin *et al.*, 2023). The thickened cell wall may contribute to enhanced salt tolerance in maize by resisting the influx of external Na^+.

ZmCIPK12 may affect the cell wall through supplementary molecular mechanisms. GO analysis indicated that some downregulated DEGs possess established or hypothesized functions related to the cell wall (Fig. 6c). We hypothesize that the thinner cell wall of *zmcipk12* plants under saline conditions can be partially attributed to the lower expression of genes, such as *Zm4CL16*, *ZmPAL7*, *ZmPME19*, *ZmPRX61* and other cell wall-related genes. Further experiments will elucidate this potential regulation.

Taken together, this study shows that ZmCIPK12 and ZmPPase4 positively regulate salt tolerance in maize and suggests a role for cell wall modification in salt tolerance in maize. This research enhances our understanding of salt tolerance mechanisms and provides gene targets for improving salt tolerance in maize.

Acknowledgements

We thank Caifu Jiang for the *zmcipk12* mutant seeds. We thank Jianfang Li, Jiaqiang Sun and Xiliu Cheng for stimulating discussions. We thank Jianan Wu from the Core Facility Platform, Institute of Crop Sciences, Chinese Academy of Agricultural Sciences (CAAS) for her assistance with TEM sample preparation and analysis. The authors acknowledge financial support from the National Key R&D Program of China (2023YFD1200500 and 2022YFD1201702), the National Natural Science Foundation of China (grant no.: 32072079), and the Agricultural Science and Technology Innovation Program of CAAS (CAAS-CSCB-202403).

Competing interests

None declared.

Author contributions

JL, XH, YW, QH, WW, JH and JZ planned and designed the research. XC and JL performed the yeast two-hybrid assays. YC constructed the ZmCIPK12 overexpression lines. Zhen Chen and JL measured the physiological indicators and performed the split-luciferase assays. JL and XH performed the phosphorylation experiments. JL performed the other experiments and analyzed the data. YG, XW, CL, RL, Zhifeng Chen and YQ grew the

plants. JL and JH wrote and revised the manuscript with contributions from the other authors.

ORCID

Jian Hua https://orcid.org/0000-0002-3777-3344
Jun Zheng https://orcid.org/0000-0002-3502-653X

Data availability

All the data supporting the findings of this study are included in this article or as Supporting Information (Figs S1–S10; Tables S1–S10).

References

Ali A, Petrov V, Yun DJ, Gechev T. 2023. Revisiting plant salt tolerance: novel components of the SOS pathway. *Trends in Plant Science* **28**: 1060–1069.

Cao Y, Liang X, Yin P, Zhang M, Jiang C. 2019. A domestication-associated reduction in K^+-preferring HKT transporter activity underlies maize shoot K^+ accumulation and salt tolerance. *New Phytologist* **222**: 301–317.

Cao Y, Zhou X, Song H, Zhang M, Jiang C. 2023. Advances in deciphering salt tolerance mechanism in maize. *Crop Journal* **11**: 1001–1010.

Chen X, Chen G, Li J, Hao X, Tuerxun Z, Chang X, Gao S, Huang Q. 2021. A maize calcineurin B-like interacting protein kinase ZmCIPK42 confers salt stress tolerance. *Physiologia Plantarum* **171**: 161–172.

Chen X, Gu Z, Xin D, Hao L, Liu C, Huang J, Ma B, Zhang H. 2011. Identification and characterization of putative CIPK genes in maize. *Journal of Genetics and Genomics* **38**: 77–87.

Chen Y, Kou X, Lian W, Hua J, Wang Y, Chen Y, Wang Q, Chai G, Bai Y. 2025. Evolution and functional characterization of *Populus* salt stress-responsive calcineurin B-like protein-interacting protein kinases. *Plant Cell Reports* **44**: 3.

Chen Z, Wang Y, Wang X, Fang T, Zhen S, Lu J, Zheng J, Fu J. 2021. Cloning and expression analysis of soluble inorganic pyrophosphatase family genes in maize (*Zea mays* L.). *Journal of Plant Genetic Resources* **22**: 455–465.

Colin L, Ruhnow F, Zhu JK, Zhao C, Zhao Y, Persson S. 2023. The cell biology of primary cell walls during salt stress. *Plant Cell* **35**: 201–217.

Dabravolski SA, Isayenkov SV. 2023. The regulation of plant cell wall organisation under salt stress. *Frontiers in Plant Science* **14**: 1118313.

De Graaf BHJ, Rudd JJ, Wheeler MJ, Perry RM, Bell EM, Osman K, Franklin FCH, Franklin-Tong VE. 2006. Self-incompatibility in *Papaver* targets soluble inorganic pyrophosphatases in pollen. *Nature* **444**: 490–493.

Eaves DJ, Haque T, Tudor RL, Barron Y, Zampronio CG, Cotton NPJ, de Graaf BHJ, White SA, Cooper HJ, Franklin FCH *et al.* 2017. Identification of phosphorylation sites altering pollen soluble inorganic pyrophosphatase activity. *Plant Physiology* **173**: 1606–1616.

Fu H, Yu X, Jiang Y, Wang Y, Yang Y, Chen S, Chen Q, Guo Y. 2023. Salt overly sensitive 1 is inhibited by clade D Protein phosphatase 2C D6 and D7 in *Arabidopsis thaliana*. *Plant Cell* **35**: 279–297.

Halfter U, Ishitani M, Zhu JK. 2000. The Arabidopsis SOS2 protein kinase physically interacts with and is activated by the calcium-binding protein SOS3. *Proceedings of the National Academy of Sciences, USA* **97**: 3735–3740.

He R, Yu G, Han X, Han J, Li W, Wang B, Huang S, Cheng X. 2017. ThPP1 gene, encodes an inorganic pyrophosphatase in *Thellungiella halophila*, enhanced the tolerance of the transgenic rice to alkali stress. *Plant Cell Reports* **36**: 1929–1942.

Liu J, Chen Z, Wang Z, Zhang Z, Xie X, Wang Z, Chai L, Song L, Cheng X, Feng M *et al.* 2021. Ectopic expression of VRT-A2 underlies the origin of *Triticum polonicum* and *Triticum petropavlovskyi* with long outer glumes and grains. *Molecular Plant* **14**: 1472–1488.

Liu X, Jiang W, Li Y, Nie H, Cui L, Li R, Tan L, Peng L, Li C, Luo J *et al.* 2023. FERONIA coordinates plant growth and salt tolerance via the phosphorylation of phyB. *Nature Plants* **9**: 645–660.

Luan S. 2009. The CBL-CIPK network in plant calcium signaling. *Trends in Plant Science* **14**: 37–42.

Ma A, Zhang D, Wang G, Wang K, Li Z, Gao Y, Li H, Bian C, Cheng J, Han Y *et al.* 2021. *Verticillium dahliae* effector VDAL protects MYB6 from degradation by interacting with PUB25 and PUB26 E3 ligases to enhance *Verticillium* wilt resistance. *Plant Cell* **33**: 3675–3699.

Ma L, Han R, Yang Y, Liu X, Li H, Zhao X, Li J, Fu H, Huo Y, Sun L *et al.* 2023. Phytochromes enhance SOS2-mediated PIF1 and PIF3 phosphorylation and degradation to promote Arabidopsis salt tolerance. *Plant Cell* **35**: 2997–3020.

Munns R, Tester M. 2008. Mechanisms of salinity tolerance. *Annual Review of Plant Biology* **59**: 651–681.

Penning BW, Shiga TM, Klimek JF, Sanmiguel PJ, Shreve J, Thimmapuram J, Sykes RW, Davis MF, McCann MC, Carpita NC. 2019. Expression profiles of cell-wall related genes vary broadly between two common maize inbreds during stem development. *BMC Genomics* **20**: 785.

Qin R, Hu Y, Chen H, Du Q, Yang J, Li WX. 2023. MicroRNA408 negatively regulates salt tolerance by affecting secondary cell wall development in maize. *Plant Physiology* **192**: 1569–1583.

Ramakrishna P, Gámez-Arjona FM, Bellani E, Martin-Olmos C, Escrig S, De Bellis D, De Luca A, Pardo JM, Quintero FJ, Genoud C *et al.* 2025. Elemental cryo-imaging reveals SOS1-dependent vacuolar sodium accumulation. *Nature* **637**: 1228–1233.

Segami S, Tomoyama T, Sakamoto S, Gunji S, Fukuda M, Kinoshita S, Mitsuda N, Ferjani A, Maeshima M. 2018. Vacuolar H^+-pyrophosphatase and cytosolic soluble pyrophosphatases cooperatively regulate pyrophosphate levels in *Arabidopsis thaliana*. *Plant Cell* **30**: 1040–1061.

Shi H, Ishitani M, Kim C, Zhu J-K. 2000. The *Arabidopsis thaliana* salt tolerance gene SOS1 encodes a putative Na^+/H^+ antiporter. *Proceedings of the National Academy of Sciences, USA* **97**: 6896–6901.

de la Torre F, Gutiérrez-Beltrán E, Pareja-Jaime Y, Chakravarthy S, Martin GB, del Pozo O. 2013. The tomato calcium sensor CBL10 and its interacting protein kinase CIPK6 define a signaling pathway in plant immunity. *Plant Cell* **25**: 2748–2764.

Wang B, Xie G, Liu Z, He R, Han J, Huang S, Liu L, Cheng X. 2019. Mutagenesis reveals that the *OsPPa6* gene is required for enhancing the alkaline tolerance in rice. *Frontiers in Plant Science* **10**: 759.

Yang Y, Guo Y. 2018. Elucidating the molecular mechanisms mediating plant salt-stress responses. *New Phytologist* **217**: 523–539.

Ye Y, Cheng Z, Yang X, Yang S, Tang K, Yu H, Gao J, Zhang Y, Leng J, Zhang W *et al.* 2025. LRM3 positively regulates stem lodging resistance by degradating MYB6 transcriptional repressor in soybean. *Plant Biotechnology Journal* **23**: 2978–2993.

Zhang F, Li L, Jiao Z, Chen Y, Liu H, Chen X, Fu J, Wang G, Zheng J. 2016. Characterization of the calcineurin B-Like (CBL) gene family in maize and functional analysis of ZmCBL9 under abscisic acid and abiotic stress treatments. *Plant Science* **253**: 118–129.

Zhang X, Li X, Zhao R, Zhou Y, Jiao Y. 2020. Evolutionary strategies drive a balance of the interacting gene products for the CBL and CIPK gene families. *New Phytologist* **226**: 1506–1516.

Zhao C, Zhang H, Song C, Zhu JK, Shabala S. 2020. Mechanisms of plant responses and adaptation to soil salinity. *The Innovation* **1**: 100017.

Zhao H, Sun N, Huang L, Qian R, Lin X, Sun C, Zhu Y. 2023. *Azospirillum brasilense* activates peroxidase-mediated cell wall modification to inhibit root cell elongation. *iScience* **26**: 107144.

Zhao S, Zhang Q, Liu M, Zhou H, Ma C, Wang P. 2021. Regulation of plant responses to salt stress. *International Journal of Molecular Sciences* **22**: 4609.

Zhou X, Li J, Wang Y, Liang X, Zhang M, Lu M, Guo Y, Qin F, Jiang C. 2022. The classical SOS pathway confers natural variation of salt tolerance in maize. *New Phytologist* **236**: 479–494.

Zhu JK. 2016. Abiotic stress signaling and responses in plants. *Cell* **167**: 313–324.

Supporting Information

Additional Supporting Information may be found online in the Supporting Information section at the end of the article.

Fig. S1 ZmCIPK12 interacts with ZmCBLs.

Fig. S2 Protein sequence multiple alignment of ZmPPase4 with its orthologous genes in Arabidopsis and rice.

Fig. S3 Subcellular localization of ZmCIPK12 and ZmPPase4.

Fig. S4 The phosphorylated peptides containing the S191 site identified by mass spectrum analysis.

Fig. S5 ZmPPase4 is phosphorylated *in vivo*.

Fig. S6 Relative expression levels of *ZmPPase4*.

Fig. S7 qRT-PCR analysis of cell-wall related genes in $WT^{B73-329}$ and *zmcipk12* plants.

Fig. S8 Decreased lignin content in *zmcipk12* seedlings under salt stress.

Fig. S9 Transcriptomic analysis of *ZmPPase4* regulated salt-responsive genes.

Fig. S10 qRT-PCR analysis of cell-wall related genes in $WT^{B73-329}$ and *zmppase4* plants.

Table S1 The list of the primers used in this study.

Table S2 Transcriptomic analysis of *ZmCIPK* family genes in B73 between control and NaCl treatment.

Table S3 305 differentially expressed genes between $WT^{B73-329}$ and *zmcipk12-1* under normal conditions.

Table S4 993 differentially expressed genes between $WT^{B73-329}$ and *zmcipk12-1* under saline conditions.

Table S5 382 up-regulated differentially expressed genes.

Table S6 532 down-regulated differentially expressed genes.

Table S7 528 differentially expressed genes between $WT^{B73-329}$ and *zmppase4-2* under normal conditions.

Table S8 512 differentially expressed genes between $WT^{B73-329}$ and *zmppase4-2* under saline conditions.

Table S9 114 up-regulated differentially expressed genes.

Table S10 348 down-regulated differentially expressed genes.

Please note: Wiley is not responsible for the content or functionality of any Supporting Information supplied by the authors. Any queries (other than missing material) should be directed to the *New Phytologist* Central Office.